Available online at www.sciencedirect.com
ScienceDirect
Trans. Nonferrous Met. Soc. China 33(2023) 1164−1177
Transactions of Nonferrous Metals Society of China
www.tnmsc.cn

Geometric size effect of Lemaitre damage model parameters of rolled CuAl5 alloy

Xiu-bin WANG, De-liang YIN, Xin-ping ZHANG

School of Materials Science and Engineering, Nanjing University of Science and Technology, Nanjing 210094, China

Received 24 November 2021; accepted 31 March 2022

Abstract: The geometric size effects (GSEs) of Lemaitre damage model parameters (the critical damage value at rupture, D_c, the strain at the damage threshold, ε_D, and the strain at rupture, ε_R) of a rolled CuAl5 alloy were evaluated using uniaxial tensile experiments and the finite element method. The results indicated the presence of size effect on the damage model parameters of the rolled CuAl5 alloy. With an increase in reduction ratio (R_r) at a constant thickness (t), D_c increased; with an increase in t at a constant R_r, D_c decreased and then increased. Both ε_D and ε_R decreased with increasing R_r and decreasing t. New models of the relationship between the damage model parameters and t were established for the three R_r values. The predicted results of the models agreed with the experimental ones. These results help to accurately predict the fracture behavior of microparts during plastic forming.

Key words: Lemaitre damage model; geometry size effect; CuAl5 alloy; reduction ratio; cold rolling

1 Introduction

With the rapid development of microelectro-mechanical systems (MEMS), small integrated devices combining mechanical and electronic parts (referred to as MEMS devices) are widely used in various fields where microparts with a geometric characteristic size at the submicron level are increasingly in demand [1,2]. Owing to their superior mechanical and processing properties, metals and their alloys are among the materials selected for microparts.

During plastic forming or service processes, the damage caused by deformation accumulates in an area with a loading force until the damage reaches a critical level where fracture occurs. This process of fracture can be quantitatively described with damage models. Several damage models have thus far been successfully applied to predicting fracture in various plastic forming technologies of metals, such as incremental forming [3], roll forming [4], hydraulic forming [5,6], deep drawing [7] and warm forming [8].

Classic damage models include three types: (1) Non-coupled damage models. Examples include the Johnson–Cook model [9], Bai−Wierzbicki model [10] and the Lou−Huh damage model [11]. The main disadvantages of these models are the difficulty of their application in complicated loading paths and large plastic strain. (2) Weakly coupled damage models. These models include the typical Gurson model [12] and the GTN model [13]. These models contain a number of material constants, some of which lack definite physical meaning and involve a difficult calibration process [14]. (3) Fully coupled damage models. These models are generally developed based on continuum damage mechanics, which average the effects of microdefects and adopt variables in macroscopic scales rather than variables concerning details of microstructures [15].

Corresponding author: De-liang YIN, Tel/Fax: +86-25-84303983, E-mail: dlyin@njust.edu.cn;
Xin-ping ZHANG, Tel/Fax: +86-25-84303983, E-mail: xpzhang@njust.edu.cn
DOI: 10.1016/S1003-6326(23)66173-4

As a fully coupled model, the Lemaitre model presents the influence of stress triaxiality on fracture in a frame of continuum damage mechanics and considers the evolution of interior defects such as the growth and coalescence of voids and their effects on the mechanical properties of materials [16,17]. SCHOWTJAK et al [18] used the Lemaitre damage model in the simulation of the rolling and cold extrusion of the 16MnCrS5 steel. KUMAR et al [19] proved the higher accuracy of the Lemaitre model in the prediction of a crack site location in single-point incremental forming. Using the Lemaitre damage model, AGHAEI and ZIAEI-RAD [20] predicted the crack initiation during the blanking process of the duplex steel DP600. The Lemaitre model has also been used to accurately predict the stamping force [21] and the occurrence of necking in deep drawing [22]. Thus, the Lemaitre damage model has a superior prediction accuracy and is widely used in various fields.

Current studies on the damage model mainly focus on the determination of model parameters and the establishment of a new model considering various stress conditions for application in complex work processes. The conventional influencing factors for parts of regular size have been extensively studied. These factors include microstructures [23], stress triaxiality and Lode angle [24,25], strain rate [26], temperature [16,27], hydrostatic pressure [27], lubricating conditions [16], and anisotropy of materials [28]. However, studies regarding the effect of specimen dimensions on damage models and their parameters have rarely been reported.

When the geometric size of a specimen decreases from regular (millimeter and above) to mesoscopic or microscopic, the grains in the deformation zone are scarce; the orientations and properties of individual grains exert striking effects on the deformation behavior [29], fracture [30,31], and surface roughness of materials [31]. For instance, the fracture strain of pure copper foil during tensile testing has been shown to decrease with a reduction in thickness [32]. On the basis of the aforementioned results, the parameters of damage models can be rationally speculated to have been influenced by the size of the specimen. Thus, a geometric size effect (GSE) might have been exerted on the parameters of the damage models. However, this speculation needs confirmation by further experiments.

This study aims to confirm the existence of GSE in damage models, explore the reason underlying the presence of GSE, and determine its concrete manifestation. For this purpose, the Lemaitre damage model was developed, with the effect of specimen thickness (t) on rolled CuAl5 alloy considered. The change rules of the damage model parameters (D_c, ε_D, and ε_R) with t and the effect of the reduction ratio (RR, R_r) on these rules were investigated. Finally, a mathematical model to describe the changes in the damage model parameters with t was established and then verified by experimental results.

2 Experimental

2.1 Specimen preparation

To avoid the influence of phase precipitation on mechanical properties, a single-phase alloy [33], the CuAl5 alloy, was used in this study. The EDS result of mold cast CuAl5 alloy is shown in Fig. 1(a), and the composition of this alloy is listed in Table 1. The cast ingots were then cold-rolled at an R_r of 30% and followed by homogenization annealing in a vacuum tube furnace at 700 °C for 4 h to eliminate cast structures and homogenize the composition. The distribution of aluminum after the aforementioned treatment is shown in Fig. 1(b), indicating the absence of component segregation. The billets were then cold-rolled at three R_r values, 30%, 50%, and 70%, and subjected to stress relief annealing to remove residual stress. Dog-bone tensile specimens with a gauge length of 7 mm, a width of 2 mm, and varying thicknesses t (0.3, 0.5, 1.0, and 2.0 mm, respectively) were cut from the interior of the rolled billets in the rolling direction (RD) (Fig. 2). The specimens were ground with $600^{\#}$ abrasive paper to remove mechanical marks.

2.2 Microstructural characterization

The microstructures were characterized by scanning electron microscopy (SEM) using the Zeiss Auriga system equipped with an Oxford Instruments electron backscatter diffraction (EBSD, HITACHI SUS1510) at an operating voltage of 12 kV and a step of 40 nm. The specimens were ground until $2000^{\#}$ abrasive paper, and then electropolished with a solution of 100 mL H_3PO_4 + 50 mL H_2O, with a voltage of 2 V at 25 °C for 40 s.

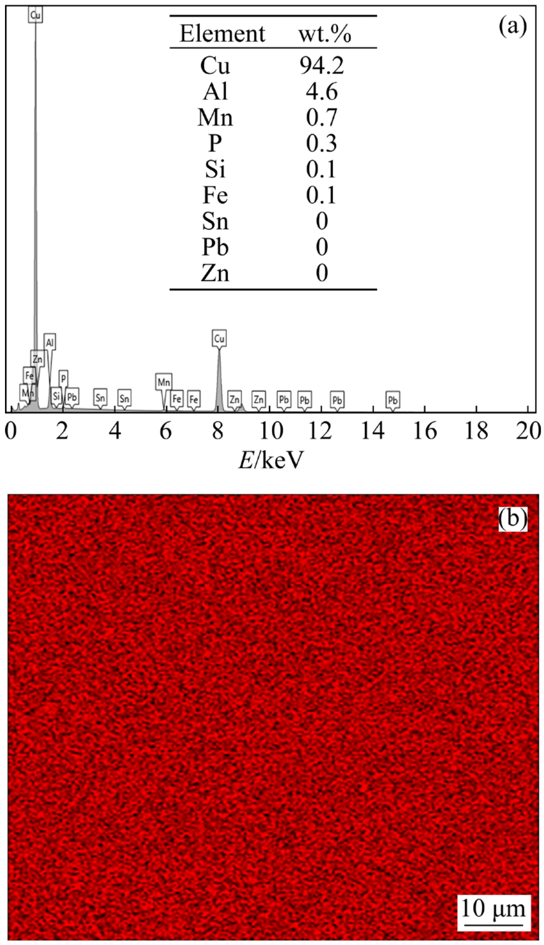

Fig. 1 SEM/EDS analysis results of CuAl5 alloy: (a) EDS spectrogram; (b) Distribution of aluminum

Table 1 Chemical composition of CuAl5 alloy (wt.%)

Cu	Al	Fe	Mn	P	Si
94.2	4.6	0.1	0.7	0.3	0.1

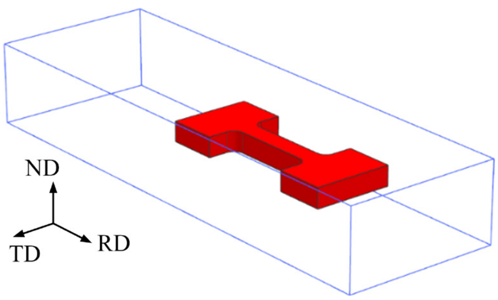

Fig. 2 Schematic of tensile specimen cut from rolled CuAl5 alloy sheet (RD: Rolling direction; ND: Normal direction; TD: Transverse direction)

2.3 Determination of Lemaitre damage model parameters

The evolution of damage ΔD in the Lemaitre damage model is given by [34]

$$\Delta D=\frac{D_{\mathrm{c}}}{\varepsilon_{\mathrm{R}}-\varepsilon_{\mathrm{D}}}\left[\frac{2}{3}(1+\gamma)+3(1-2\gamma)\left(\frac{\sigma_{\mathrm{H}}}{\overline{\sigma}}\right)^{2}\right]\cdot\left(\overline{\varepsilon}_{0}+\overline{\varepsilon}^{\mathrm{Pl}}\right)^{2n}\Delta\overline{\varepsilon}^{\mathrm{Pl}} \tag{1}$$

where D_{c}, ε_{R}, and ε_{D} are the damage parameters; γ, σ_{H}, $\overline{\varepsilon}_{0}$, $\Delta\overline{\varepsilon}^{\mathrm{Pl}}$, $\overline{\varepsilon}^{\mathrm{Pl}}$, and n represent the Poisson's ratio, hydrostatic stress, initial pre-strain, plastic strain increment, equivalent plastic strain, and strain-hardening exponent, respectively.

Originally, determined by the repetitive loading–unloading tensile test proposed by Lemaitre [17,35], the three parameters D_{c}, ε_{D}, and ε_{R} correspond to the critical damage value at rupture, the strain at the damage threshold, and the strain at rupture, respectively. In 2019, VERMA and SAXENA [36] showed that high-precision Lemaitre damage model parameters can be obtained using uniaxial tensile experiments. In addition, the help document of the commercial software Simufact Forming (Chapter 13 Damage and kinematic hardening) also introduces the use of uniaxial tensile experiments to obtain Lemaitre damage model parameters. The damage model parameters were thus obtained using uniaxial tensile experiments in this study.

The gauge length direction and the thickness direction of the tensile test specimens were parallel to the RD and normal direction (ND), respectively. For the specimens with t of 0.3 and 0.5 mm, tensile tests were performed on a customized device, which consisted of a guide rail, a digital pull–push force gauge (maximum load of 200 N, and error range of 0.5%), a stepping motor, and its control system. For the specimens with t of 1.0−2.0 mm, the tests were performed using a Shimadzu UTM/CMT 5000 Universal Tester (Shimadzu, Japan). The initial strain rate was $1\times10^{-3}\,\mathrm{s}^{-1}$, and five specimens were used for each condition. The fracture morphology was observed by SEM, and the reduction in area was calculated using SEM images.

Digital image correlation using the software Vic-2D was performed to study the strain distribution of the specimen during tensile testing. White paint was uniformly sprayed on the surface of the specimen, and an atomizer was used to spray ink dots on the surface to form randomly distributed speckle images. An advanced industrial camera was used to take photos at a rate of one frame per second. The standard deviation (Stdev) reflects a statistic that measures the dispersion of a dataset relative to its mean. When the strain distribution is highly inhomogeneous (that is, the values of the strain are farther from the mean), the data set shows a large deviation. Thus, the Stdev of strains was used to describe the inhomogeneity of deformation.

2.4 Finite element analysis

To verify the damage model, the tensile process was simulated by the finite element method (FEM) using the software Abaqus/Explicit. The Lemaitre damage model was implanted as a Vumat subroutine. The implantation details of the model in Abaqus are found in the literature [37−39]. When the damage D of an element reached D_c, the element was deleted. The element type was C3D8R. The grid sizes in the thickness direction and other directions were $t/10$ and 0.1, respectively.

The constitutive model is an important parameter for FEM. The typical flow stress curves of the rolled CuAl5 alloy are presented in Fig. 3. With reference to the literature [40] and the characteristics of these curves, the Ludwik law and the Voce model were selected as candidate constitutive models.

Ludwik's law is expressed as [41]

$$\sigma = \sigma_0 + k\varepsilon^n \tag{2}$$

Voce's law is given by [42]

$$\sigma=\sigma_0+A[1-\exp(-m\varepsilon)] \tag{3}$$

where σ_0, k, and ε denote the yield stress, strength coefficient, and plastic strain, respectively; A and m represent the material constants.

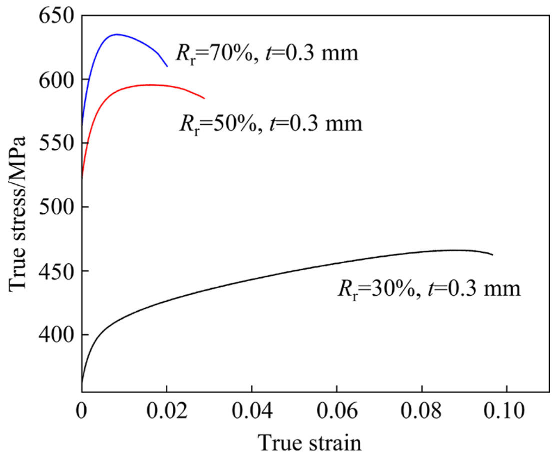

Fig. 3 Strain−stress curves of rolled CuAl5 alloy

3 Results

3.1 Microstructures and fracture morphology of rolled CuAl5 alloy

The microstructures of the rolled CuAl5 alloy in the rolling direction (normal direction section) is shown in Fig. 4. Coarse grains containing twins with an average grain size of 21.2 μm and relatively random orientations were observed with an R_r of 30%. With an increase in R_r, the average grain size decreased, accompanied by a preferred orientation. When R_r=50%, the ⟨110⟩ crystal directions of many grains were tilted toward the transverse direction (TD), and when R_r=70%, the $\langle 2\bar{1}1\rangle$ crystal directions of more grains were tilted toward TD with a smaller average grain size of 8.75 μm.

Figure 5 presents the SEM images of the fracture morphologies of tensile specimens. At the same R_r, both the dimple size (Fig. 5) and the

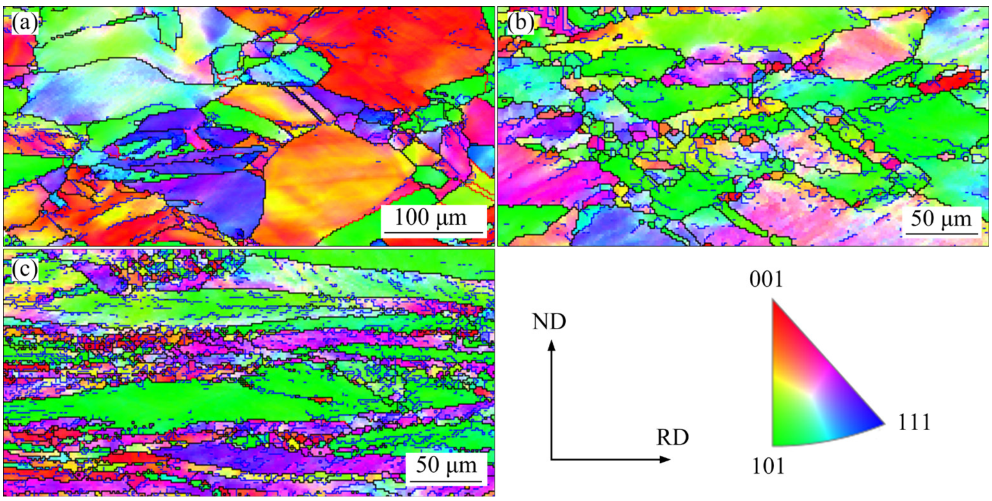

Fig. 4 EBSD results for CuAl5 specimens rolled at different R_r values: (a) 30%; (b) 50%; (c) 70%

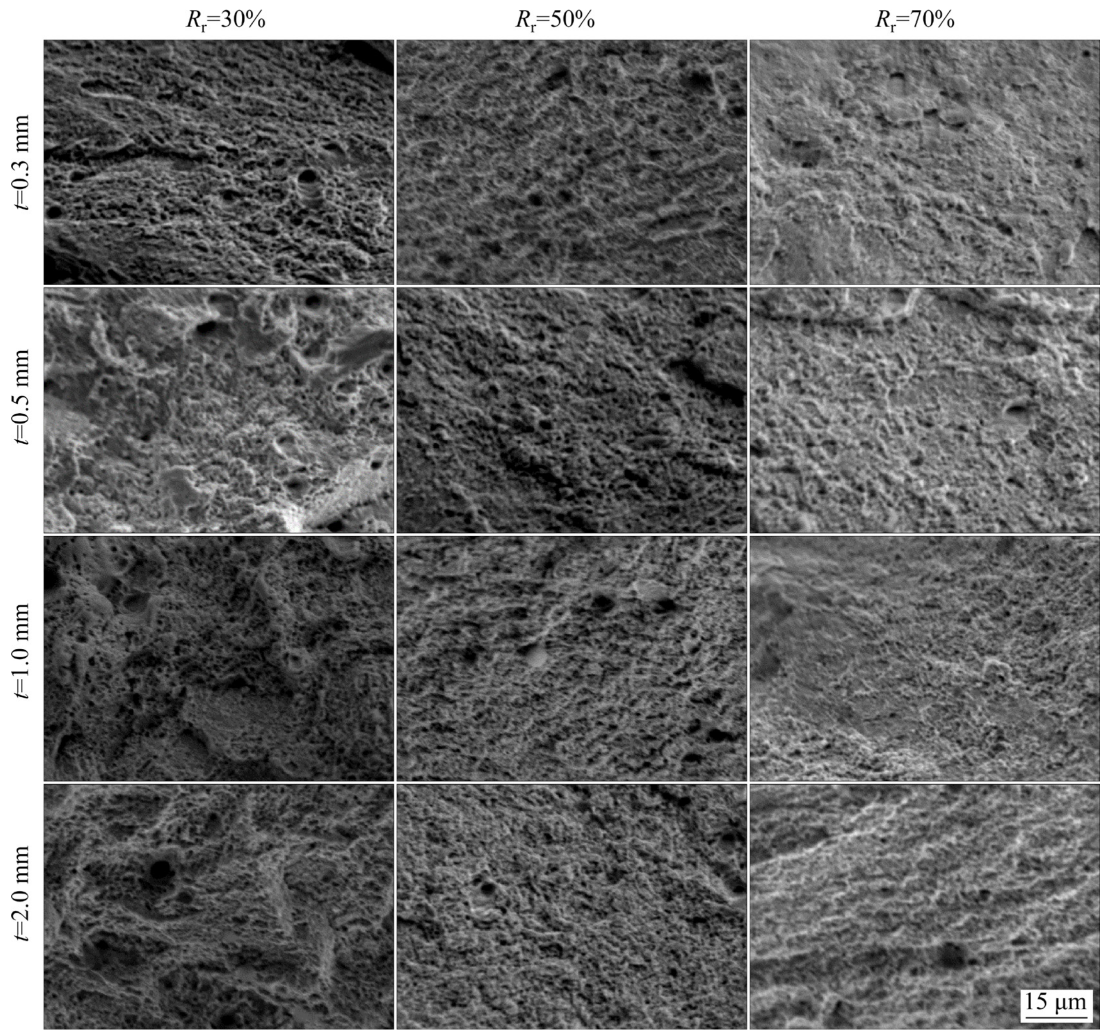

Fig. 5 SEM fracture morphologies of CuAl5 tensile specimens at different R_r and t values

reduction in area (Fig. 6) increased with the increase in t. However, at the same t, the reductions in area and dimple size decreased with an increase in R_r. Thus, when R_r=30% and t=2 mm, the maximum area reduction (45%) was reached, and when R_r=70% and t=0.3 mm, the minimum reduction in area (16.6%) was obtained.

3.2 Constitutive models for CuAl5 alloy

The constitutive model that accurately describes the stress–strain relationship of a material is the basis of FEM. To accurately simulate the tensile fracture process of the CuAl5 alloy, the constitutive model of the alloy with different t values needs to be established. When t=0.5 mm, the fitting results for the flow stress curves of the rolled CuAl5 alloy, obtained using Voce's law and Ludwik's law, are illustrated in Fig. 7. When t=0.5 mm, the flow stress of the specimen rolled at

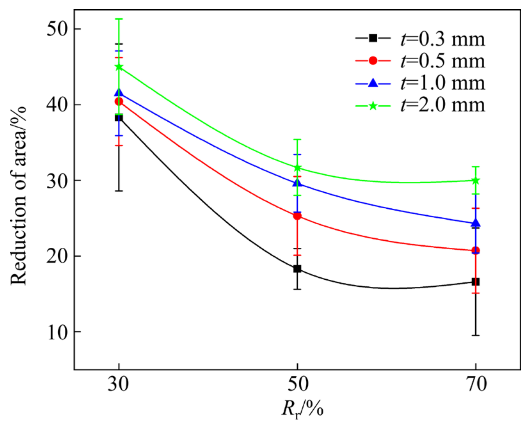

Fig. 6 Reductions of area of CuAl5 tensile fracture specimens at different R_r and t values

R_r=30% followed Ludwik's law, whereas that of the specimens rolled at R_r=50%−70% followed Voce's law. The same method was used to fit the flow stress curves of the specimens with other R_r and t values. The models are listed in Table 2.

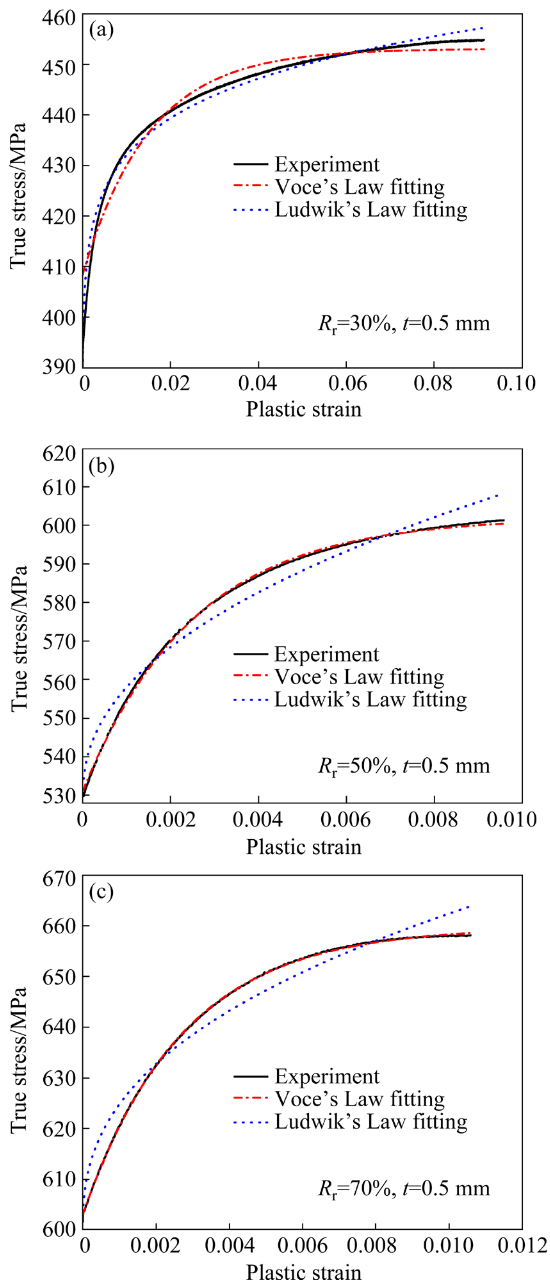

Fig. 7 Fitting of flow stress curves generated using two constitutive models for rolled CuAl5 alloy at different R_r values (t =0.5 mm): (a) R_r=30%; (b) R_r=50%; (c) R_r=70%

3.3 Lemaitre damage model of rolled CuAl5 alloy and its verification

The Lemaitre damage model parameters D_c, ε_D, and ε_R for specimens with different R_r and t values are listed in Table 3. These parameters were used to simulate the tensile testing of the CuAl5 alloy. Simulated force–displacement curves were obtained and compared with the experimental ones (Fig. 8). The errors in the plastic deformation stage between the simulation and experimental results were smaller than ±5%, indicating that the Lemaitre damage model can accurately predict the damage and fracture of the rolled CuAl5 alloy in tensile testing.

Table 2 Constitutive models for rolled CuAl5 alloy

R_r/%	t/mm	Constitutive model	R^2
30	0.3	σ=336.1+228.6$\varepsilon^{0.24}$	0.9971
	0.5	σ=381.2+239$\varepsilon^{0.31}$	0.9981
	1.0	σ=373.6+256.1$\varepsilon^{0.25}$	0.9958
	2.0	σ=380.9+239.1$\varepsilon^{0.24}$	0.9948
50	0.3	σ=523.3+69.4[1−exp(−363ε)]	1.00
	0.5	σ=529.7+71.3[1−exp(−359ε)]	1.00
	1.0	σ=579.9+46.3[1−exp(−342.9ε)]	1.00
	2.0	σ=576.9+61.8[1−exp(−297.9ε)]	0.9999
70	0.3	σ=564.6+77[1−exp(−361.3ε)]	1.00
	0.5	σ=607.7+62[1−exp(−344.1ε)]	0.9999
	1.0	σ=620.5+65.4[1−exp(−342.3ε)]	1.00
	2.0	σ=627.3+78.8[1−exp(−270.3ε)]	1.00

R^2 is squares sum of correlation coefficients

Table 3 Lemaitre damage model parameters for CuAl5 alloy

R_r/%	t/mm	D_c	ε_D	ε_R
30	0.3	0.0055	0.0872	0.0924
	0.5	0.0106	0.1039	0.1120
	1.0	0.0188	0.1479	0.1683
	2.0	0.0156	0.1531	0.1695
50	0.3	0.0230	0.0155	0.0263
	0.5	0.0288	0.0218	0.0483
	1.0	0.0402	0.0216	0.0652
	2.0	0.0319	0.0307	0.0851
70	0.3	0.0346	0.0118	0.0255
	0.5	0.0416	0.0143	0.0377
	1.0	0.0487	0.0187	0.0585
	2.0	0.0435	0.0214	0.0791

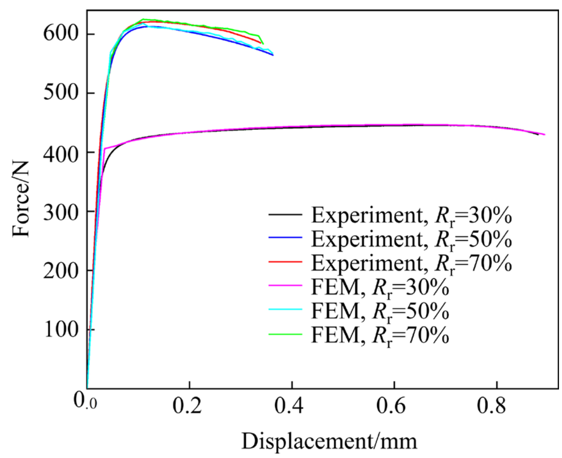

Fig. 8 Comparison of force−displacement curves between FEM simulation and experimental results for tensile testing with different R_r values (t=0.5 mm)

4 Discussion

4.1 Effects of R_r and t on ε_D and ε_R of rolled CuAl5 alloy

The changes in ε_D and ε_R with t and R_r are shown in Fig. 9. ε_D and ε_R exerted GSEs, and both increased with an increase in t. When the grain size was constant, the thin specimen had a small number of grains in the thickness direction, resulting in the activation of several slip systems during deformation. The characteristics of individual grains (shape, size, and direction) affected the fracture mode of the material and the compatibility of the deformation [43].

(1) Fracture mode

When $t\geq1.0$ mm, the fracture was dominated by the ductile fracture mode. When $t<1.0$ mm, the fracture changed to the brittle fracture mode (Fig. 5). Thus, fracture was more likely to occur in the specimen with a smaller t than in the specimen with a larger t. The higher the toughness of the material was, the larger the dimples were [44]. The dimple size of these specimens is proportional to t (Fig. 5), indicating that the fracture strain of the rolled CuAl alloy increased with an increase in t.

(2) Coordinated deformation

The number of grains in the thickness direction increased with an increase in t. The increase in the number of grains contributed to the improvement in the coordination between the grains during deformation. This finding was proved by the Stdev of the strain distribution during the tensile process (Fig. 10). At constant R_r, the greater the t was, the smaller the Stdev of the strain distribution was. This finding indicates that the uniformity of the strain distribution increased with an increase in t. These comprehensive effects induced increases in ε_D and ε_R with t.

The gap between ε_D and ε_R, which also showed a GSE, increased with an increase in t. The size of microvoids in materials was not reduced as t decreased, and the influence of microvoids in a thinner specimen became more significant [45]. The defects caused stress concentration, leading to strain localization, and the earlier occurrence of fracture (Fig. 10). This prompted an increase in the difference between ε_D and ε_R with an increase in t.

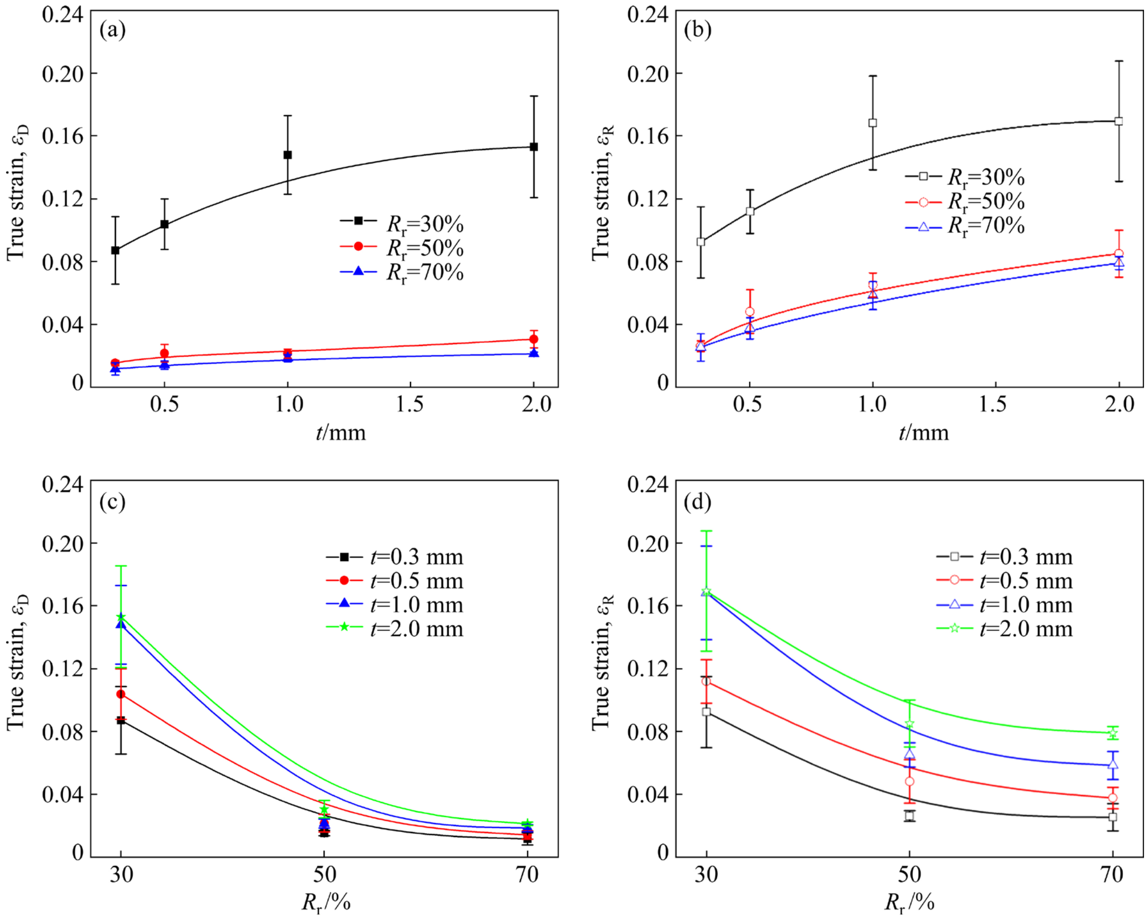

Fig. 9 Changes in ε_D and ε_R of CuAl alloy with t and R_r: (a) ε_D with t; (b) ε_R with t; (c) ε_D with R_r; (d) ε_R with R_r

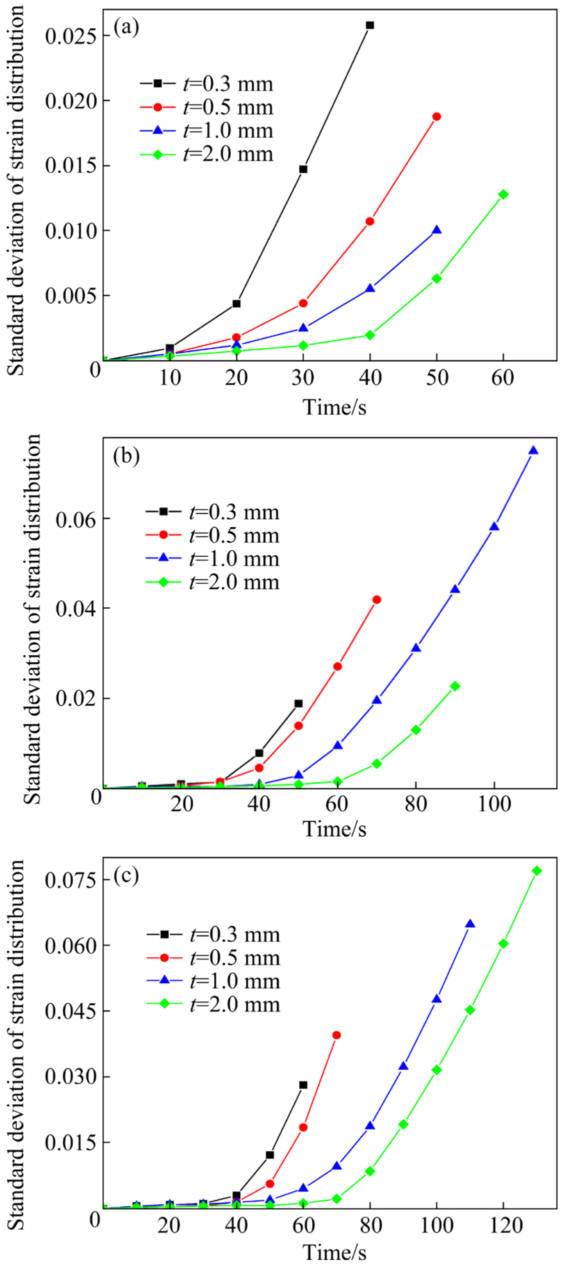

Fig. 10 Standard deviation of strain distribution of tensile specimens with different R_r values based on Vic-2D analysis: (a) R_r=30%; (b) R_r=50%; (c) R_r=70%

The grain size decreased with an increase in R_r (Fig. 4). If the t remains constant and R_r increases, the increased number of grains in the thickness direction leads to an improvement in the deformation coordination. Therefore, ε_D and ε_R theoretically increased with an increase in R_r. However, both ε_D and ε_R decreased with an increase in R_r (Fig. 9(b)), which was mainly attributed to two factors. (1) As shown in Fig. 11, when the specimen is necked, the slope of the standard deviation–time curve increases with the increase of R_r, indicating

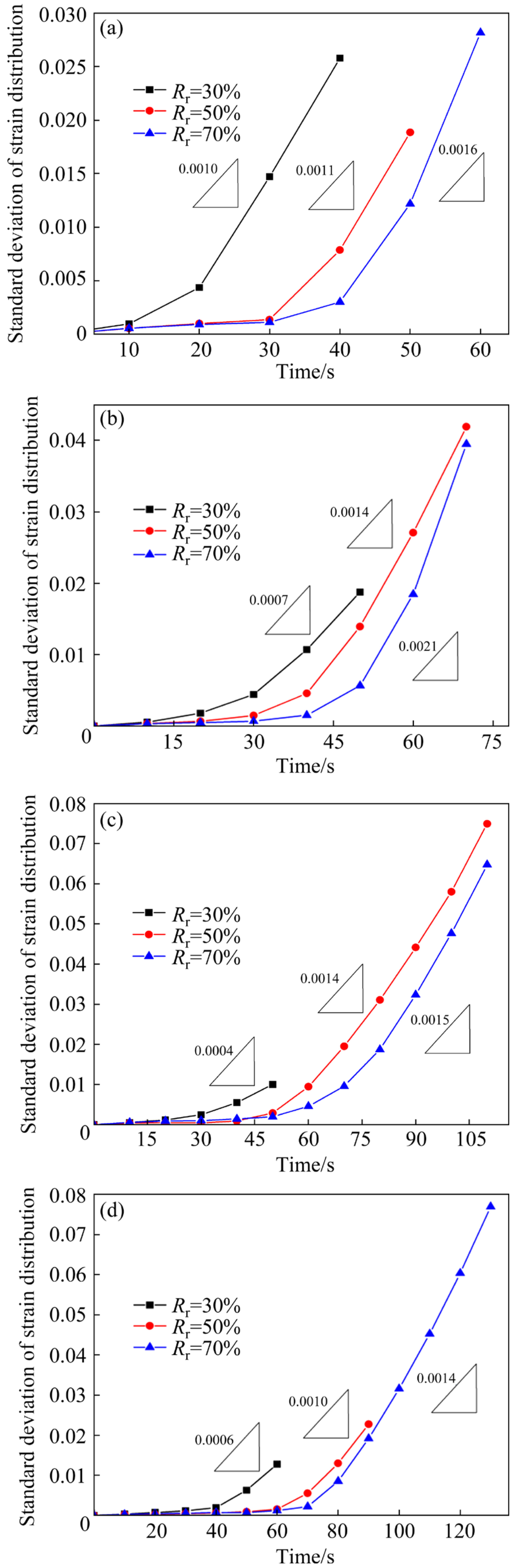

Fig. 11 Standard deviation of strain distribution of tensile specimens with different t values based on Vic-2D analysis: (a) t=0.3 mm; (b) t=0.5 mm; (c) t=1.0 mm; (d) t=2.0 mm

that the strain inhomogeneity of the specimen deformed increases at this stage, and the stress concentration in a specimen rolled at higher R_r becomes more significant. This occurrence can cause the specimen to fracture more easily. (2) Apart from deformation twinning (Fig. 4), rolling also increased the dislocation density. According to the study by WANG et al [46], when the dislocation slip is severely restricted, the local internal stress tends to increase, and tensile strength and necking can more easily occur. Moreover, deformation twinning is depleted with an increase in pre-strain [47], which also leads to a decrease in ε_D.

4.2 Effects of R_r and t on D_c of rolled CuAl5 alloy

As shown in Fig. 12, D_c shows a generally increasing trend with an increase in t; that is to say, D_c exerts a GSE.

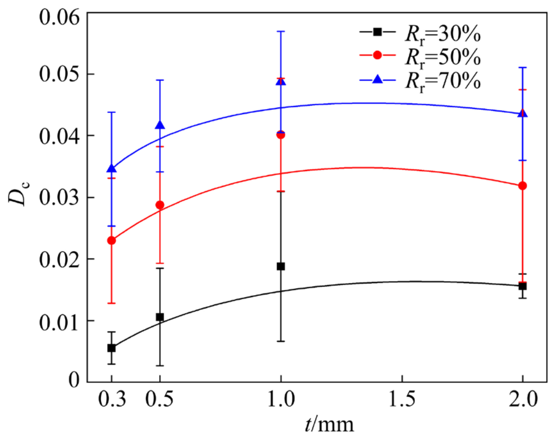

Fig. 12 Relationships between D_c and t of CuAl5 alloy rolled at different R_r values

D_c depends on the ratio of fracture stress (FTS, σ_f) to ultimate tensile stress (UTS, σ_b), given that $D_c=1-\sigma_f/\sigma_b$. At constant R_r, the grain size is basically the same, and the thin specimen has only few grains in thickness direction. Correspondingly, only a few slip systems are activated during deformation, and the interaction between dislocations weakens. Thus, the UTS and FTS of the specimen increase with the increase of t (Fig. 13). Simultaneously, when t is small, the individual grain characteristics (shape, size, and direction) affect the deformation behavior of the material. Thus, the smaller the t is, the earlier the occurrence of fracture in the specimen is. Figure 10 shows that the smaller the t is, the earlier the non-uniform deformation during tensile testing is, and the more severe the necking deformation is. Thus, the ratio of FTS to UTS decreases as t increases.

The increase in D_c with t can also be explained by fracture mechanics. When the material reaches UTS, microcracks are generated inside the material. Three types of crack are formed in the material, types I, II, and III. The type I crack is used as an example for the sake of discussion. The material exhibits characteristic resistance to fracture, K_{IC}, known as "fracture toughness". When the applied loading is such that $K_I \geq K_{IC}$, then the crack grows, and fracture eventually occurs. K_I represents the stress intensity factor [48].

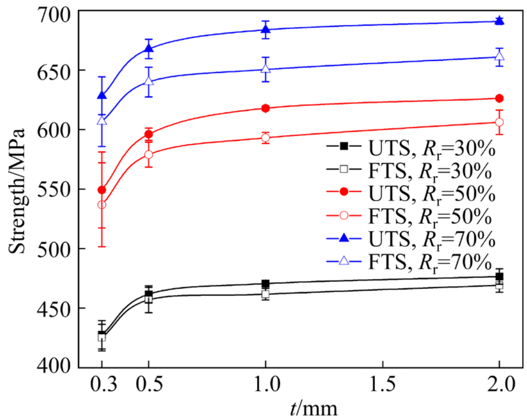

Fig. 13 Relationships between strengths (UTS and FTS) and t of CuAl5 alloy rolled at different R_r values

Fundamental to the understanding of elastic–plastic fracture is the determination of the size and shape of the crack tip plastic zone. When the t of the specimen is larger, the tip near the crack tends to be in a plane strain state, and the plastic zone size r_p is expressed as follows if we introduce a polar coordinate system (r_p and θ) as illustrated in Fig. 14:

$$r_p = \max\left\{\frac{K_I^2}{2\pi\sigma_0^2}\cos^2\left(\frac{\theta}{2}\right)\left[(1-2\gamma)+\sin\left(\frac{\theta}{2}\right)\right]^2, \frac{K_I^2}{2\pi\sigma_0^2}2\cos^2\left(\frac{\theta}{2}\right)\sin^2\left(\frac{\theta}{2}\right)\right\} \tag{4}$$

When t is reduced to a certain value, the tip near the crack tends to be under plane stress, and r_p is given by

$$r_p = \frac{K_I^2}{2\pi\sigma_0^2}\left[\cos\left(\frac{\theta}{2}\right)\left(1+\sin\left(\frac{\theta}{2}\right)\right)\right]^2 \tag{5}$$

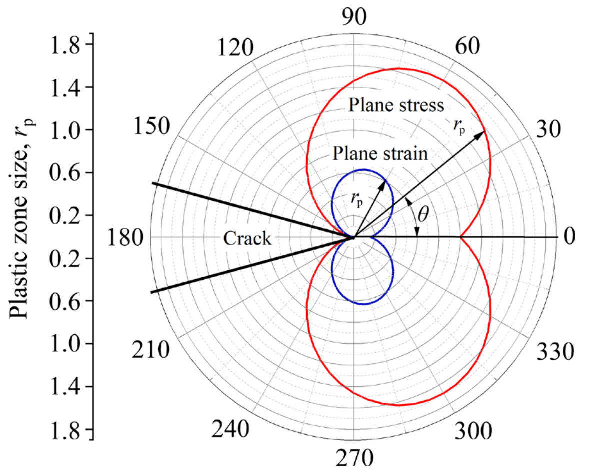

Fig. 14 Sizes and shapes of plane stress and plane strain plastic zones ($K_I^2/(2\pi\sigma_0^2)$ is assumed to be 1)

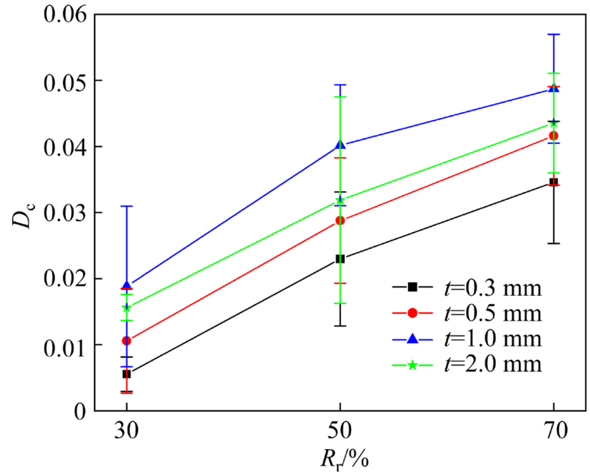

Fig. 15 Relationship between D_c and R_r of CuAl5 alloy with different t values

As shown in Fig. 14, the size of the plastic zone under plane strain is smaller than that under plane stress. Thus, the plastic zone of the thick specimen is smaller than that of the thin specimen. Owing to the existence of the plastic zone near the tip of the crack, the effective length of the crack increases from the initial crack length a to a+r_p. K_I increases from $Y\sigma\sqrt{\pi a}$ to $Y\sigma\sqrt{\pi(a+r_p)}$, where Y is the shape factor. Therefore, the plastic zone generated at the tip of the crack significantly increases the stress intensity. The plastic zone under plane strain is smaller than that under plane stress; thus, K_I under plane stress (the thin specimen) is larger than that under plane strain (the thick specimen). The K_I of the thin specimen can reach K_{IC} faster than that of the thick specimen; consequently, the crack growth rate of the thin specimen is higher than that of the thick specimen. Correspondingly, the voids in the thin specimen are not fully developed, and the void fraction of the fracture cross-sectional area of the thin specimen is smaller than that of the thick specimen, as shown in Fig. 5. D_c denotes the critical void area fraction in the cross-sectional area of the fracture [17,35]. Thus, D_c increases with t.

As shown in Fig. 15, the D_c of the specimens with the same t increases with R_r. As earlier mentioned, D_c depends on the ratio of FTS to UTS. In the current study, the UTS and FTS of the rolled CuAl5 alloy increased with the increase in R_r (Fig. 16), consistent with the conclusions of KIM et al [49] and JIANG et al [50]. Increase in R_r led to grain refinement, apparent preferred orientation,

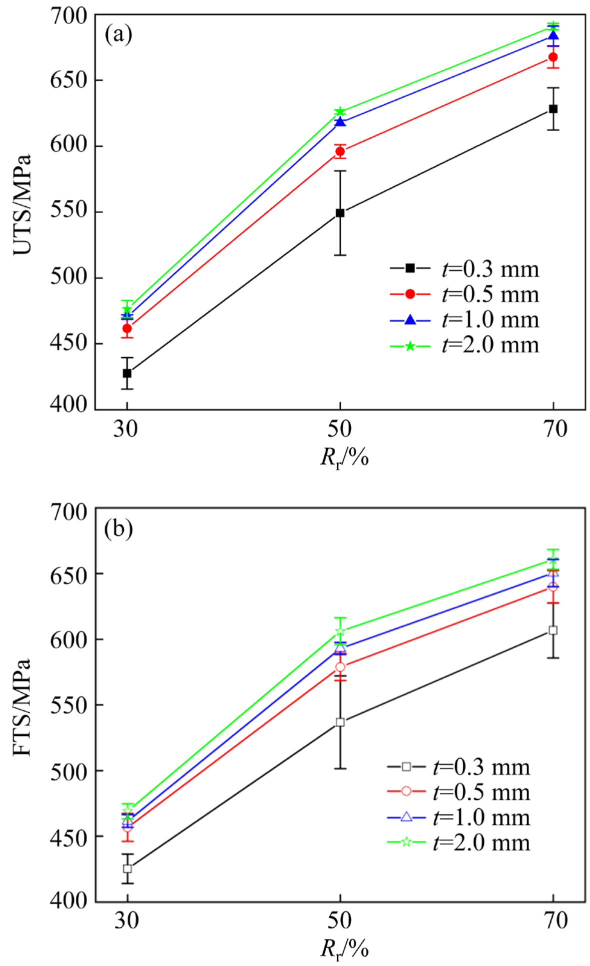

Fig. 16 Relationship between strength and R_r of CuAl5 alloy with different t values: (a) UTS vs R_r; (b) FTS vs R_r

and increases in the grain boundary and dislocation density, thereby increasing UTS and FTS. As shown in Fig. 11, the change rate in the strain standard deviation of the specimen with time during necking (the slope of the latter part of the curves) increases with R_r. In the present study, the stress concentration of the specimen roller at a higher R_r was more significant during necking, leading to a faster reduction in nominal stress. Thus, the increase in FTS with R_r was lower than that in UTS. Correspondingly, the D_c of the specimens at a constant t increased with the increase in R_r (Fig. 16).

4.3 Mathematical model of GSE of Lemaitre damage model parameters

GSE is an important research field in microforming technology. To quantitatively describe GSE, a model between the geometric size and the mechanical properties of the material needs to be established. Currently, the GSE model mainly focuses on the flow stress of the material [51−54], and the mathematical model of the change in damage model parameters with the dimension of the specimen has not been reported. In the present study, a model was proposed for the quantification of the effect of t on the damage model parameters of the rolled CuAl5 alloy.

In accordance with the relationships between the parameters (D_c, ε_D, and ε_R) and t in Figs. 9 and 12, the D_c can be estimated using the quadratic equation; ε_D and ε_R can be estimated using the cubic equation. The fitting results are presented in Fig. 17.

The Nonlinear Surface Fit module in the software Origin was used to calculate the coefficients in these models, and the results are listed in Table 4. An R^2 value of exactly +1 indicates a perfect fit; thus, on the basis of the derived R^2 values, the fitted relationships were found to be in good agreement with the experimental data.

To verify the accuracy of these models, the predicted results were compared with the experimental ones (Table 5). The maximum relative error was 2.31%, less than 10%, and thus fell within the acceptable margin of error for use in the industry. Thus, the predicted results agreed with the experimental ones.

To verify the reliability of these models, the Lemaitre damage models of the rolled CuAl5 alloy with t value of 0.76 mm were established using a previously described method. The experimental and predicted parameters are compared in Table 6. The maximum relative error was 9.06%, less than 10%, which fell within the acceptable error range for use in the industry. Through these verifications, the predicted results for the damage model parameters agreed with the experimental ones.

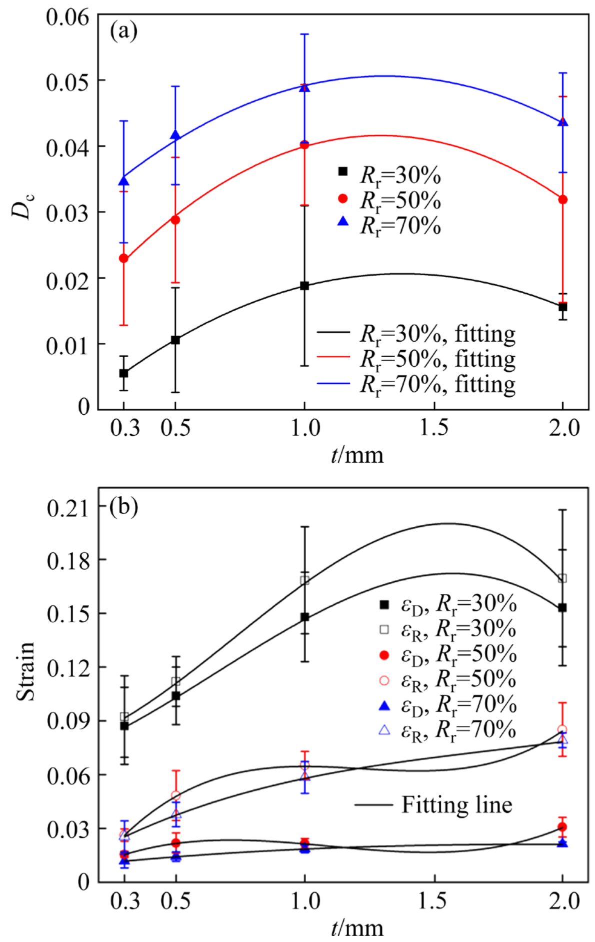

Fig. 17 Variations in fitting results of Lemaitre damage model parameters with t: (a) D_c; (b) ε_D and ε_R

Table 4 Geometric size effect models of D_c, ε_D and ε_R in Lemaitre damage model for rolled CuAl5 alloy

R_r/%	Geometric size effect model	R^2
30	D_c=0.0358t−0.013t^2−0.004	1.00
	ε_D=0.044t+0.071t^2−0.036t^3+0.068	0.9978
	ε_R=0.027t+0.121t^2−0.056t^3+0.074	0.9978
50	D_c=0.05t−0.0193t^2−0.0093	0.9867
	ε_D=0.096t−0.1t^2+0.03t^3−0.005	0.9980
	ε_R=0.25t−0.212t^2+0.058t^3−0.031	0.9995
70	D_c=0.0391t−0.015t^2+0.025	0.9515
	ε_D=0.017t−0.006t^2+0.001t^3+0.007	0.9954
	ε_R=0.09t−0.042t^2+0.008t^3+0.002	0.9991

R^2 is squared sum of correlation coefficients

Table 5 Experimental and predicted of D_c, ε_R and ε_R

R_r/%	t/mm	D_c-Exp.	D_c-Pre.	RE. of D_c/%	ε_R-Exp.	ε_R-Pre.	RE. of ε_R/%	ε_D-Exp.	ε_D-Pre.	RE. of ε_D/%
30	0.3	0.0055	0.0055	0.00	0.0924	0.0915	0.97	0.0872	0.0863	1.03
	0.5	0.0106	0.0106	0.00	0.1120	0.1109	0.98	0.1039	0.1029	0.96
	1.0	0.0188	0.0188	0.00	0.1683	0.1667	0.95	0.1479	0.1465	0.95
	2.0	0.0156	0.0156	0.00	0.1695	0.1678	1.00	0.1531	0.1515	1.05
50	0.3	0.0230	0.0225	2.17	0.0263	0.0261	0.76	0.0155	0.0154	0.65
	0.5	0.0288	0.0294	2.08	0.0483	0.0478	1.04	0.0218	0.0216	0.92
	1.0	0.0402	0.0399	0.75	0.0652	0.0646	0.92	0.0216	0.0214	0.93
	2.0	0.0319	0.0320	0.31	0.0851	0.0843	0.94	0.0307	0.0304	0.98
70	0.3	0.0346	0.0354	2.31	0.0255	0.0253	0.78	0.0118	0.0117	0.85
	0.5	0.0416	0.0408	1.92	0.0377	0.0374	0.80	0.0143	0.0142	0.70
	1.0	0.0487	0.0492	1.03	0.0585	0.0579	1.03	0.0187	0.0185	1.07
	2.0	0.0435	0.0435	0.00	0.0791	0.0783	1.01	0.0214	0.0212	0.93

Exp.: Experimental; Pre.: Predicted; RE.: Absolute value of relative error

Table 6 Comparison of experimental values of Lemaitre damage model parameters of rolled CuAl5 alloy with thickness of 0.76 mm and prediction results of models in Table 4

R_r/%	D_c			ε_R			ε_D		
	Exp.	Pre.	RE./%	Exp.	Pre.	RE./%	Exp.	Pre.	RE./%
30	0.0160	0.0157	1.88	0.1216	0.1262	3.78	0.1329	0.1402	5.49
50	0.0331	0.0361	9.06	0.0241	0.0234	2.90	0.0586	0.0616	5.12
70	0.0504	0.0461	8.53	0.0181	0.0167	7.73	0.0539	0.0495	8.16

Exp.: Experimental; Pre.: Predicted; RE.: Absolute value of relative error

5 Conclusions

(1) The Lemaitre damage model parameters, D_c, ε_D, and ε_R of the rolled CuAl5 alloy exert a geometric size effect.

(2) At constant reduction ratio R_r, D_c increased as t increased from 0.3 to 1.0 mm and decreased as t increased to 2.0 mm. When R_r values were 30%, 50% and 70%, the maximum D_c values were 0.0156, 0.0319, and 0.0435, respectively.

(3) When the sample thickness (t) was constant, D_c increased as R_r increased from 30% to 70%. When t was 0.3, 0.5, 1.0, and 2.0 mm, the maximum D_c values were 0.0346, 0.0416, 0.0487, and 0.0435, respectively, at a constant R_r of 70%.

(4) Both ε_D and ε_R decreased with increasing R_r and decreasing t. ε_D and ε_r reached the maximum values when R_r was 30%, and t was 2.0 mm; meanwhile, the minimum values were obtained when R_r was 70%, and t was 0.3 mm.

(5) Models of the relationship between the damage model parameters and t were established for three R_r values. The maximum relative error between the experimental and predicted parameters was 9.06%.

(6) As t or R_r decreased, the uniform deformation time of the tensile specimen was shortened, and the deformation inhomogeneity during necking increased. The increase in D_c with t is further explained by fracture mechanics; a larger effective crack length in the thin specimens leads to a lower D_c than that of the thick ones.

Acknowledgments

The authors are grateful for the financial supports from the National Natural Science Foundation of China (No. 51675283).

References

[1] MISHRA M K, DUBEY V, MISHRA P M, KHAN I. MEMS technology: A review [J]. Journal of Engineering Research and Reports, 2019, 4: 1−24.

[2] ZHU Jian-xiong, LIU Xin-miao, SHI Qiong-feng, HE Tian-yi-yi, SUN Zhong-da, GUO Xin-ge, LIU Wei-xin, SULAIMAN O B, DONG Bo-wei, LEE Cheng-kuo. Development trends and perspectives of future sensors and MEMS/NEMS [J]. Micromachines, 2020, 11: 7.

[3] MIRNIA M J, SHAMSARI M. Numerical prediction of failure in single point incremental forming using a phenomenological ductile fracture criterion [J]. Journal of

Materials Processing Technology, 2017, 244: 17−43.

[4] MIRNIA M J, VAHDANI M, SHAMSARI M. Ductile damage and deformation mechanics in multistage single point incremental forming [J]. International Journal of Mechanical Sciences, 2018, 136: 396−412.

[5] BAI Y, WIERZBICKI T. A comparative study of three groups of ductile fracture loci in the 3D space [J]. Engineering Fracture Mechanics, 2015, 135: 147−167.

[6] HASHEMI S J, NAEINI H M, LIAGHAT G H, TAFTI R A. Prediction of bulge height in warm hydroforming of aluminum tubes using ductile fracture criteria [J]. Archives of Civil and Mechanical Engineering, 2015, 15: 19−29.

[7] LIU Hong-sheng, YANG Yu-ying, YU Zhong-qi, SUN Zhen-zhong, WANG Yong-zhi. The application of a ductile fracture criterion to the prediction of the forming limit of sheet metals [J]. Journal of Materials Processing Technology, 2009, 209: 5443−5447.

[8] MORCHHALE A, BADRISH A, KOTKUNDE N, SINGH S K, KHANNA N, SAXENA A, NIKHARE C. Prediction of fracture limits of Ni–Cr based alloy under warm forming condition using ductile damage models and numerical method [J]. Transactions of Nonferrous Metals Society of China, 2021, 31: 2372−2387.

[9] MAGALHÃES D C C, KLIAUGA A M, SORDI V L. Flow behavior and fracture of Al−Mg−Si alloy at cryogenic temperatures [J]. Transactions of Nonferrous Metals Society of China, 2021, 31: 595−608.

[10] BAI Y, WIERZBICKI T. A new model of metal plasticity and fracture with pressure and Lode dependence [J]. International Journal of Plasticity, 2008, 24: 1071−1096.

[11] DONG Guo-jiang, CHEN Zhi-wei, YANG Zhuo-yun, FAN Bo-cheng. Comparative study on forming limit prediction of AA7075-T6 sheet with M−K model and Lou−Huh criterion [J]. Transactions of Nonferrous Metals Society of China, 2020, 30: 1463−1477.

[12] GURSON A L. Continuum theory of ductile rupture by void nucleation and growth: Part I—Yield criteria and flow rules for porous ductile media [J]. Journal of Engineering Materials and Technology, 1977, 99: 2−15.

[13] TENG Bu-gang, YUAN Shi-jian, CHEN Zeng-tao, JIN Xue-run. Plastic damage of T-shape hydroforming [J]. Transactions of Nonferrous Metals Society of China, 2012, 22: s294−s301.

[14] CAO T S. Models for ductile damage and fracture prediction in cold bulk metal forming processes: A review [J]. International Journal of Material Forming, 2017, 10: 139−171.

[15] ZHANG Kai, BADREDDINE H, SAANOUNI K. Ductile fracture prediction using enhanced CDM model with Lode angle-dependency for titanium alloy Ti−6Al−4V at room temperature [J]. Journal of Materials Processing Technology, 2020, 277: 116462.

[16] HEIDARI A, GHASSEMI A, ATRIAN A. A numerical and experimental investigation of temperature effects on the formability of AA6063 sheets using different ductile fracture criteria [J]. The International Journal of Advanced Manufacturing Technology, 2020, 106: 2595−2611.

[17] LEMAITRE J. A Continuous damage mechanics model for ductile fracture [J]. Transactions of the Asme Journal of Engineering Materials & Technology, 1985, 107: 83−89.

[18] SCHOWTJAK A, WANG Shu-han, HERING O, CLAUSMEYER T, LOHMAR J, SCHULTE R, OSTWALD R, HIRT G, TEKKAYA A E. Prediction and analysis of damage evolution during caliber rolling and subsequent cold forward extrusion [J]. Production Engineering, 2020, 14: 33−41.

[19] KUMAR A, SINGH A K, SHRIVASTVA A, MISHRA S, NARASIMHAN K. Failure prediction in incremental sheet forming based on Lemaitre damage model [J]. Journal of Physics: Conference Series, 2018, 1063: 12152.

[20] AGHAE I, ZIAEI-RAD S. A micro mechanical study on DP600 steel under tensile loading using Lemaitre damage model coupled with combined hardening [J]. Materials Science and Engineering A, 2020, 772: 138774.

[21] GUTKNECHT F, ISIK K, CLAUSMEYER T, TEKKAYA E. Comparison of gurson and lemaitre model in the context of blanking simulation of a high strength steel [C]//Proceedings of the XIV International Conference on Computational Plasticity: Fundamentals and applications. CIMNE, 2017: 163−173.

[22] CHALAL H, ABED-MERAIM F. Numerical predictions of the occurrence of necking in deep drawing processes [J]. Metals, 2017, 7: 455.

[23] LU Ding-ding, LI Jin-feng, NING Hong, MA Peng-cheng, CHEN Yong-lai, ZHANG Xu-hu, Zhang Kai, LI Jian-mei, ZHANG Rui-feng. Effects of microstructure on tensile properties of AA2050-T84 Al−Li alloy [J]. Transactions of Nonferrous Metals Society of China, 2021, 31: 1189−1204.

[24] GAO Xiao-sheng, ZHANG Gui-hua, ROE C. A study on the effect of the stress state on ductile fracture [J]. International Journal of Damage Mechanics, 2009, 19: 75−94.

[25] LI Wen-chao, LIAO Fang-fang, ZHOU Tian-hua, ASKES H. Ductile fracture of Q460 steel: Effects of stress triaxiality and Lode angle [J]. Journal of Constructional Steel Research, 2016, 123: 1−17.

[26] ROTH C C, MOHR D. Effect of strain rate on ductile fracture initiation in advanced high strength steel sheets: Experiments and modeling [J]. International Journal of Plasticity, 2014, 56: 19−44.

[27] KHAN A S, LIU Hao-wen. Strain rate and temperature dependent fracture criteria for isotropic and anisotropic metals [J]. International Journal of Plasticity, 2012, 37: 1−15.

[28] DONG Liang, LI Shu-hui, HE Ji. Ductile Fracture Initiation of Anisotropic Metal Sheets [J]. Journal of Materials Engineering and Performance, 2017, 26: 3285−3298.

[29] MA Zhen-wu, PENG Xuan, WANG Chun-ju, CAO Zi-yang. Modeling of material deformation behavior in micro-forming under consideration of individual grain heterogeneity [J]. Transactions of Nonferrous Metals Society of China, 2020, 30: 2994−3005.

[30] CARPINTERI A, CORRADO M, GONG B, PERDONÒ P. Experimental evidence and numerical simulation of size effects on the ductile fracture of metallic materials [J]. International Journal of Fracture, 2018, 211: 43−59.

[31] MENG B, FU M W. Size effect on deformation behavior and ductile fracture in microforming of pure copper sheets considering free surface roughening [J]. Materials & Design, 2015, 83: 400−4012.

[32] FURUSHIMA T, TSUNEZAKI H, MANABE K I, ALEXSANDROV S. Ductile fracture and free surface roughening behaviors of pure copper foils for micro/meso-scale forming [J]. International Journal of Machine Tools and Manufacture, 2014, 76: 34−48.

[33] OKAMOTO H, SCHIESINGER M E, MUELLER E M. ASM Metals HandBook Volume 3− Alloy Phase Digram [M]. ASM International, 2016.

[34] LEE S W, POURBOGHRAT F. Finite element simulation of the punchless piercing process with Lemaitre damage model

[J]. International Journal of Mechanical Sciences, 2005, 47: 1756−1768.

[35] LEMAITRE J. A course on damage mechanics [M]. Verlag: Springer, 1996.

[36] VERMA A, SAXENA R K. Determination of Lemaitre damage parameters for DP590 steel using Teacher−Learner based optimization [J]. Journal of Physics: Conference Series, 2019, 1240: 12101.

[37] LEE S, IM Y D, MATSUMOTO R, UTSUNOMIYA H. Strength and electrical conductivity of Cu−Al alloy sheets by cryogenic high-speed rolling [J]. Materials Science and Engineering A, 2021, 799: 139815.

[38] VAZ M, MUÑOZ-ROJAS P A, CARDOSO E L, TOMIYAMA M. Considerations on parameter identification and material response for Gurson-type and Lemaitre-type constitutive models [J]. International Journal of Mechanical Sciences, 2016, 106: 254−265.

[39] SOYARSLAN C, RICHTER H, BARGMANN S. Variants of Lemaitre's damage model and their use in formability prediction of metallic materials [J]. Mechanics of Materials, 2016, 92: 58−79.

[40] TRIEU K, WANG Xiu-bin, ZHANG Xin-ping. The effect of size on the mechanical properties of rolled specimen: Predictions and experimental evaluation [J]. Materials Research Express, 2019, 6: 115801.

[41] ADEAGBO M O, LAM H F, NI Yi-qing. A Bayesian methodology for detection of railway ballast damage using the modified Ludwik nonlinear model [J]. Engineering Structures, 2021, 236: 112047.

[42] VOCE E. The relationship between stress and strain for homogeneous deformation [J]. Journal of the Institute of Metals, 1948, 74: 537−562.

[43] YANG H K, CAO K, HAN Y, WEN M, GUO J M, TAN Z L, LU J, LU Y. The combined effects of grain and sample sizes on the mechanical properties and fracture modes of gold microwires [J]. Journal of Materials Science & Technology, 2019, 35: 76−83.

[44] QIN Wen-bo, LI Jian-sheng, LIU Yao-yao, KANG Jia-jie, ZHU Li-na, SHU Deng-feng, PENG Peng, SHE Ding-shun, MENG De-zhong, LI Yu-sheng. Effects of grain size on tensile property and fracture morphology of 316L stainless steel [J]. Materials Letters, 2019, 254: 116−119.

[45] ZHAO Y H, GUO Y Z, WEI Q, DANGELEWICZ A M, XU C, ZHU Y T, LANGDON T G, ZHOU Y Z, LAVERNIA E J. Influence of specimen dimensions on the tensile behavior of ultrafine-grained Cu [J]. Scripta Materialia, 2008, 59: 627−630.

[46] WANG Bo, CHEN Xian-hua, PAN Fu-sheng, MAO Jian-jun, FANG Yong. Effects of cold rolling and heat treatment on microstructure and mechanical properties of AA 5052 aluminum alloy [J]. Transactions of Nonferrous Metals Society of China, 2015, 25: 2481−2489.

[47] HWANG J K. Revealing the small post-necking elongation in twinning-induced plasticity steels [J]. Journal of Materials Science, 2020, 55: 8285−8302.

[48] ZEHNDER A T . Linear elastic stress analysis of 2D cracks [M]. Netherlands: Springer, 2012.

[49] KIM M T, PARK T M, BAIK K H, CHOI W S, HAN J. Effects of cold rolling reduction ratio on microstructures and tensile properties of intercritically annealed medium-Mn steels [J]. Materials Science and Engineering A, 2019, 752: 43−54.

[50] JIANG Chen-chen, GAO Qiu-zhi, ZHANG Hai-lian, LIU Zi-yun, LI Hui-jun. Microstructure and mechanical properties of 4Al alumina-forming austenitic steel after cold-rolling deformation and annealing [J]. Materials, 2020, 13: 2767.

[51] CHEN F, CHEN S, DONG X H, LI C Y, HONG X T, ZHANG X P. Size effects on tensile strength of aluminum–bronze alloy at room temperature [J]. Materials & Design, 2015, 85: 778−784.

[52] DONG Xue-hua, HONG Xiang-ting, CHEN Fei, SANG B R, YU W, ZHANG Xin-ping. Effects of specimen and grain sizes on compression strength of annealed wrought copper alloy at room temperature [J]. Materials & Design, 2014, 64: 400−406.

[53] PENG Lin-fa, LIU Fang, NI Jun, LAI Xin-min. Size effects in thin sheet metal forming and its elastic–plastic constitutive model [J]. Materials & Design, 2007, 28: 1731−1736.

[54] TRIEU K, WANG Xiu-bin, YIN De-liang, ZHANG Xin-ping. Effects of stacking fault energy and reduction ratio on mechanical properties geometry size effect of cold-rolled pure Cu and CuAl alloy [J]. Journal of Alloys and Compounds, 2021, 883: 160783.

轧制态 CuAl5 合金 Lemaitre 损伤模型参数的几何尺寸效应

王秀宾，尹德良，张新平

南京理工大学 材料科学与工程学院，南京 210094

摘　要：通过单轴拉伸实验与有限元模拟相结合，研究轧制态 CuAl5 合金 Lemaitre 损伤模型参数(临界损伤值 D_c、损伤阈值处的应变 ε_D 和断裂时的应变 ε_R)的几何尺寸效应。结果表明，轧制态 CuAl5 合金损伤模型参数的确存在尺寸效应。在相同试样厚度(t)时，D_c 随轧制压下率(R_r)的增加而增加，在相同 R_r 下，随 t 的增加先减小后增加；随着 R_r 的增加或 t 的减小，ε_D 和 ε_R 都呈增加趋势。此外，建立对应 3 种 R_r 值的损伤模型参数与 t 之间关系的数学模型，并通过试验验证模型预测的准确性。研究结果有利于微型零件塑性变形时断裂行为的预测。

关键词：Lemaitre 损伤模型；几何尺寸效应；CuAl5 合金；压下率；冷轧

(Edited by Bing YANG)